# Semiconductive $K_2MSbS_3(SH)$ (M = Zn, Cd) Featuring One-Dimensional $^1_\infty[M_2Sb_2S_6(SH_2)]^{4-}$ Chains

Xian Zhang,[†] Na Yi,[‡] Roald Hoffmann,[#] Chong Zheng,[§] Jianhua Lin,[*,†] and Fuqiang Huang[*,†,‡]

[†]Beijing National Laboratory for Molecular Sciences and State Key Laboratory of Rare Earth Materials Chemistry and Applications, College of Chemistry and Molecular Engineering, Peking University, Beijing 100871, P. R. China

[‡]State Key Laboratory of High Performance Ceramics and Superfine Microstructure, Shanghai Institute of Ceramics, Chinese Academy of Sciences, Shanghai 200050, P. R. China

[#]Department of Chemistry and Chemical Biology, Cornell University, Ithaca, New York 14853, United States

[§]Department of Chemistry and Biochemistry, Northern Illinois University, DeKalb, Illinois 60115, United States

Ⓢ *Supporting Information*

**ABSTRACT:** We synthesized two one-dimensional compounds $K_2MSbS_3(SH)$ (M = Zn, Cd) at 473 K, using thiourea as reactive flux. The compounds crystallize in the triclinic space group $P\bar{1}$. Their structures feature one-dimensional $^1_\infty[M_2Sb_2S_6(SH_2)]^{4-}$ double chains along the crystallographic $a$ axis. The $^1_\infty[M_2Sb_2S_6(SH_2)]^{4-}$ double chains are composed of $[M_2Sb_2S_8(SH)_2]^{8-}$ eight-membered rings. Similar band gaps of the two compounds, $E_g = 2.75$ eV for $K_2ZnSbS_3(SH)$ and $E_g = 2.71$ eV for $K_2CdSbS_3(SH)$, were obtained from optical absorption measurements, which are consistent with theoretical calculations. The analysis of density of states indicates that the valence band maximum and conduction band minimum consist mainly of S−3p orbitals and Sb−5p orbitals, respectively.
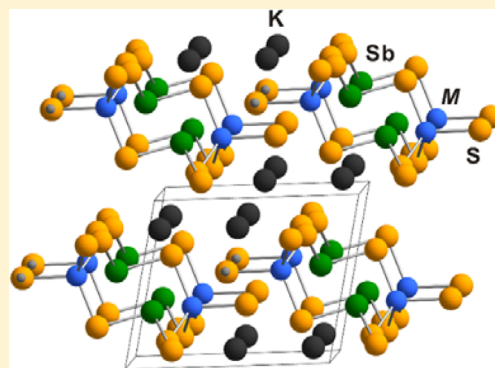
## INTRODUCTION

Multicomponent materials can easily integrate the advantages of the constituent parts and offer researchers greater opportunities and capabilities to tune their properties for desired functions.[1−4] Because of the different bonding and packing possibilities, multicomponent components may present different structural/functional units.[1−5] Therefore, these multicomponent materials with different structural/functional units can be tailored to have desired physical properties. For instance, the combination of the $^2_\infty[La_2O_2]^{2+}$ and $^2_\infty[Cu_2S_2]^{2-}$ structural/functional units can create transparent conducting LaOCuS (two-dimensional (2D), $E_g = 3.1$ eV),[6−10] the combination of the $^2_\infty[Bi_2O_2]^{2+}$ and $^2_\infty[SBi_2]^{4+}$ structural/functional units can create photoelectric $Bi_2O_2S$ (2D, $E_g = 1.12$ eV),[11,12] and the combination of $^1_\infty[ZrS_5]^{6-}$ and $^1_\infty[Zn_6S_9]^{6-}$ structural/functional units can generate multiband $Ba_6Zn_6ZrS_{14}$ (one-dimensional (1D), $E_g = 1.78$ eV, 2.50 and 2.65 eV).[1] Hence, it makes sense for us to explore these materials.

The II−VI group semiconductors play important roles in solar cells (e.g., CdTe thin-film solar cells, CdQ quantum dot multipolaron solar cells),[13,14] light-emitting diodes, photoluminescence, and lasers devices.[15] Reduction of the dimensions of the II−VI group semiconductors can lead to special properties that cannot be achieved in bulk materials. The traditional way to reduce the dimensions of II−VI group semiconductors is nanocrystallization. While the process may give rise to unexpected novel properties, there has been less

work focusing on the structural reduction of dimensions.[16−19] Additional components in a multicomponent material with low dimensions can break the connection between building blocks. This research direction motivates the present work.

To "dilute" the MS-based building blocks (M = Zn, Cd), metal ions with high ionicity such as alkali metal ions are chosen. However, from the viewpoint of electronic structure, the introduction of alkali metal ions may enlarge the band gap due to the reduction of dimensions, the consequent decrease of band dispersion,[18] and the larger electronegativity difference between the cations and anions.[20] Hence, another component should be added to tune the electronic structure. Antimony sulfide is a semiconductor with band gap of 1.7 eV.[21] In the band structure of $Sb_2S_3$, the S-3p and Sb-5s orbitals build up the valence band maximum (VBM), while the conduction band minimum (CBM) is mainly composed of Sb-5p states. Therefore, a transition may occur between the Sb-5s states in VBM to Sb-5p states in CBM, allowing SbS-based building blocks to dominate the band structure, in turn tuning the band structure of the MS-based materials (M = Zn, Cd). In addition, the lone pairs of Sb atoms may be stereochemically active, which can further reduce the dimensions of desired materials.

One of the most efficient ways to synthesize chalcogenides is the reactive flux method, due to the milder reaction condition

(i.e., relatively low reaction temperature) than traditional high-temperature solid-state reactions. The well-known reactive flux used for synthesizing chalcogenides is a series of alkali metal polychalcognides $A_2Q_{n+1}$ (A = Na, K, Rb, Cs; Q = S, Se, Te; $n \geq 0$).[22] They have low melting points and can gradually release the Q component for the reactions. Recently, we found that similar to the $A_2Q_{n+1}$ series, thiourea can also gradually release S at higher temperature than its melting point (182 °C).[12,23−25] Therefore, it can be used as another reactive flux as well. In addition, the amine group of thiourea can efficiently coordinate to metal ions and increase its solubility.

For the reasons stated above, we used the thiourea as reactive flux to explore new sulfides that contain the MS- (M = Zn, Cd) and SbS-based building blocks, and successfully synthesized two isostructural compounds, namely, $K_2ZnSbS_3(SH)$ and $K_2CdSbS_3(SH)$. The structure features 1D $^1_\infty[M_2Sb_2S_6(SH_2)]^{4-}$ double chains along the $a$ axis. The $^1_\infty[M_2Sb_2S_6(SH_2)]^{4-}$ double chains are composed of $[M_2Sb_2S_8(SH)_2]^{8-}$ eight-membered rings. Optical absorption results indicate that the two compounds have similar band gap. Density functional theory (DFT) calculations were performed to analyze the electronic structure of the compounds. The computational results reveal that the Sb-5p states dominate the CBM. Photoluminescence properties of the two compounds were also measured.

## ■ EXPERIMENTAL SECTION

**Reagents.** All starting materials were obtained from Sinopharm Chemical Reagent Beijing Co., Ltd., and used without further purification: (i) potassium hydroxide, AR, 96%; (ii) $M(CH_3COO)_2 \cdot 2H_2O$ (M = Zn, Cd), AR, 99%; (iii) antimony powder, 99.7%; (iv) thiourea, AR, 99%; (v) sulfur powder, sublimed, 99.5%. All reagents were kept in a drybox prior to use.

**Synthesis of $Sb_2S_3$.** Antimony sulfide ($Sb_2S_3$) was synthesized via solid-state reaction at 773 K of a mixture of S powder and Sb powder. A mixture of Sb powder (2.435 g, 20 mmol) and S powder (0.962 g, 30 mmol) was loaded into a carbon-coated fused silica tube. The tube was then flame-sealed under vacuum ($1 \times 10^{-3}$ mbar), and heated slowly to 773 K with a programmable furnace. The reaction was kept at this temperature for 20 h and then quenched in air. Before use, the as-synthesized $Sb_2S_3$ was then mechanically crushed into a fine powder by using a high-speed planetary ball-milling device. The ball milling of the antimony sulfide was performed in a sealed jar filled with Ar. The ball-to-powder weight ratio was ∼15:1, and the rotation speed was 1500 rpm. To avoid excessive heating during the milling, each 30 min of milling was followed by a 15 min pause. After the milling, the jar was opened in an Ar-protected glovebox.

**Synthesis of $K_2MSbS_3(SH)$ Single Crystals (M = Zn, Cd).** A mixture of starting materials of 15 g of KOH, 2.5 mmol of $M(CH_3COO)_2 \cdot 2H_2O$ (M = Zn, Cd), 2.5 mmol of $Sb_2S_3$ fine powder, and 0.1 mol of thiourea were weighed and ground uniformly. Then the mixture was transferred into a Teflon-lined steel autoclave. The synthesis was performed at 473 K for 4 d. Afterward, the autoclave was pulled out of the hot oven and allowed to cool to room temperature. The products were taken out and transferred into 100 mL of deionized water, followed by ultrasonic washing several times and drying by acetone. Finally, the pale yellow $K_2ZnSbS_3(SH)$ and $K_2CdSbS_3(SH)$ crystals were obtained, with yields of 47% and 78% (based on the 2.5 mmol of $M(CH_3COO)_2 \cdot 2H_2O$), respectively.

**Single-Crystal X-ray Crystallography.** High-quality crystals of $K_2MSbS_3(SH)$ (M = Zn, Cd) were chosen from the as-prepared samples and mounted on a glass fiber for single-crystal X-ray diffraction. Data collection was performed on an Agilent Super Nova diffractometer equipped with mirror-monochromatized Mo Kα radiation at 180 K. The structures of the two compounds were solved with direct methods built into the program SHELXS and refined with the full-matrix least-squares method using the SHELXTL-97

program.[26] The crystal data and the structure refinement details for $K_2MSbS_3(SH)$ (M = Zn, Cd) are summarized in Table 1. Selected bond lengths and angles are listed in Table S1.

**Table 1. Crystallographic Data and Details of the Structure Refinements for $K_2MSbS_3(SH)$ (M = Zn, Cd)[a]**

| formula | $K_2ZnSbS_3(SH)$ | $K_2CdSbS_3(SH)$ |
|---|---|---|
| $F_w$ (g·mol$^{-1}$) | 394.6 | 441.6 |
| crystal system | triclinic | triclinic |
| space group | $P\bar{1}$ | $P\bar{1}$ |
| $a$ (Å) | 7.0488(6) | 7.1985(7) |
| $b$ (Å) | 7.3276(7) | 7.512(1) |
| $c$ (Å) | 8.6885(6) | 8.874(1) |
| $\alpha$ (deg) | 77.898(7) | 77.37 (1) |
| $\beta$ (deg) | 89.114(6) | 89.086(9) |
| $\gamma$ (deg) | 86.961(7) | 87.49(1) |
| $V$ (Å$^3$) | 438.17(6) | 467.8(1) |
| Z | 2 | 2 |
| crystal color | pale yellow | pale yellow |
| $\rho_c$ (g·cm$^{-3}$) | 2.991 | 3.135 |
| $\mu$ (mm$^{-1}$) | 7.627 | 6.853 |
| $F(000)$ | 368 | 404 |
| $R_{int}$ | 0.028 | 0.021 |
| $R_1$ $[I > 2\sigma(I)]$ | 0.046 | 0.029 |
| $wR_2$ (all data)[a] | 0.132 | 0.088 |
| GOF | 1.137 | 1.085 |

[a]$R_1 = \sum||F_o| - |F_c||/\sum F_o$. $wR_2 = [\sum w(F_o^2 - F_c^2)^2/\sum w(F_o^2)^2]^{1/2}$.

**Powder X-ray Diffraction.** The as-synthesized crystal samples were ground into fine powder before use. Phase purity of the powder samples was checked by powder X-ray diffraction performed on a Bruker D2 Phaser diffractometer equipped with a monochromatized source of Cu Kα radiation ($\lambda$ = 0.15406 nm) at 4 kW (40 kV, 100 mA). The patterns were recorded in a slow-scanning mode with $2\theta$ from 10° to 70° at a scan rate of 1.2°/min. Simulated patterns were generated by using the GSAS program[27] and the CIF file of the refined single crystal structure.

**Ultraviolet−Visible Diffuse Reflectance Spectroscopy.** The solid-state ultraviolet−visible (UV−vis) light diffuse-reflectance spectra of the fine powders of $K_2MSbS_3(SH)$ (M = Zn, Cd) were measured on a UV-4100 spectrophotometer operating from 1200 to 250 nm at room temperature. The fine powders of the as-synthesized samples were spread on a compacted base of $BaSO_4$ powder (100% reflectance standard). The generated reflectance-versus-wavelength data were used to measure the band gap of the as-synthesized samples. The reflectance data were converted to absorbance data by using the Kubelka−Munk equation.[28]

**Fourier Transform Infrared Spectroscopy.** Before use, the two compounds were ground into fine powders and dried in a vacuum oven at 60 °C overnight. Afterward, the fine powders were ground with KBr and pressed into thin slices. FT-IR spectral measurements were performed using a Magna-IR 750 instrument operating from 4000 to 1500 cm$^{-1}$ at room temperature.

**X-ray Photoelectron Spectroscopy.** The XPS spectra of the two compounds were obtained with an Axis Ultra spectrometer to investigate the oxidation states of the Zn/Cd, Sb, and S. The spectra were collected for the C 1s, Zn 2p, Cd 3p, Sb 3d, and S 2s regions, and the binding energies corrected against the C 1s reference of 284.5 eV.

**Thermogravimetric Measurements.** The crystal samples are dried overnight in a vacuum oven at 60 °C to remove the absorbed water. The thermogravimetric measurements were performed on Q600SDT thermogravimetric analyzer. The operating temperature ranged from 20 to 800 °C with the heating rate of 10 °C/min. Nitrogen, with flow rate of 100 mL/min, was used as the protective gas.

**Photoluminescence Spectroscopy.** The fine powders of the two compounds were loaded in silica cuvettes. A Hitachi F-7000 fluorescence spectrophotometer was used to establish the photoluminescent properties of the two samples. The operation range was from 200 to 800 nm at room temperature.

**Electronic Structure Calculation.** DFT) computations were performed using the Vienna Ab Initio Simulation Package (VASP).[29−31] The Perdew−Burke−Ernzerhof (PBE) version of the generalized gradient approximation (GGA)[32] was used to describe the exchange correlation functional, and the projector augmented wave (PAW)[33] method was used in the present work. Here, the cutoff energy of plane wave was chosen at 350 eV. For the density of states (DOS) calculations, a $6 \times 6 \times 6$ Monkhorst−Pack grid was used for the primitive cell and $4 \times 4 \times 4$ k-points for the conventional cell.

## ■ RESULTS AND DISCUSSION

**Synthesis and Crystal Structure Description.** Using the reactive flux (thiourea) method, assisted by KOH (mineralizer), we synthesized two new compounds, namely, $K_2ZnSbS_3(SH)$ and $K_2CdSbS_3(SH)$. Scanning electron microscopy (SEM) images of well-defined $K_2MSbS_3(SH)$ crystals are presented in Figure S1a,c in Supporting Information. The presence of K, Zn/Cd, Sb, and S was confirmed by semiquantitative energy dispersive X-ray analysis (EDX) as shown in Figure S1b,d in Supporting Information. The average atomic ratio was 2.2/1/1/4.1 for $K_2ZnSbS_3(SH)$ and 1.9/1/1.1/3.8 for $K_2CdSbS_3(SH)$.

The two isostructural compounds crystallize in the triclinic $P\bar{1}$ space group, as depicted in Figure 1. The crystal structures
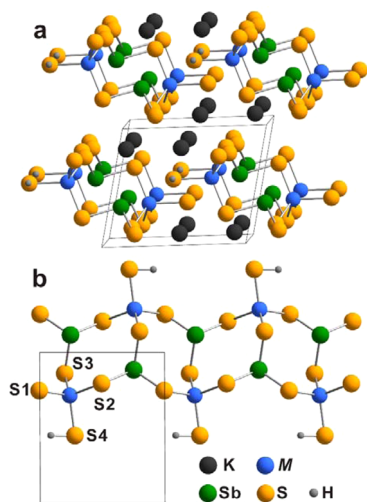


**Figure 1.** (a) Schematic diagrams of the structure of $K_2MSbS_3(SH)$ (M = Zn, Cd) viewed along the $a$ axis. (b) The $^1_\infty[M_2Sb_2S_6(SH_2)]^{4-}$ double chain.

contain two independent K sites (K1, K2), one independent M (M = Zn, Cd) site, one independent Sb site, and four independent S sites (S1−S4; S4 is bonded to a hydrogen atom). $K_2MSbS_3(SH)$ is composed of unique 1D $^1_\infty[M_2Sb_2S_6(SH_2)]^{4-}$ double chains along the $a$ axis (Figure 1). The $K^+$ ions separate the double chains from each other. The $[M_2Sb_2S_8(SH)_2]^{8-}$ eight-membered rings, as illustrated in Figure S2 in Supporting Information, serve as the building blocks of the $^1_\infty[M_2Sb_2S_6(SH_2)]^{4-}$ double chain (Figure 1b). Each of the $[M_2Sb_2S_8(SH)_2]^{8-}$ eight-membered rings is built up by two $[MS_3(SH)]^{5-}$ tetrahedra and two $[SbS_3]^{3-}$ pyramids via corner sharing (Figure S2 in Supporting Information). Each M atom is coordinated to four sulfur atoms to form distorted $MS_4$

tetrahedra. The Zn−S (S1−S3) distances are in the range of 2.335(2)−2.372(2) Å, while the Zn−S4 distance is 2.349(2) Å. The Cd−S (S1−S3) distances are in the range of 2.511(6)−2.547(6) Å, while the Cd−S4 distance is 2.521(6) Å. The Zn−S and Cd−S distances are comparable to those in the reported structures (2.366 Å for Zn−S distance in $Na_2ZnS_2$,[34] 2.545 Å for average Cd−S distance in $K_2Cd_3S_4$[16,18]). The average Sb−S distances of $K_2ZnSbS_3(SH)$ and $K_2CdSbS_3(SH)$ are 2.420(2) Å and 2.414(6) Å, respectively. There are two different types of K atoms in the crystal structure; both of them are located in distorted monocapped trigonal prism, as shown in Figure S3 in Supporting Information.

The crystal structure determination naturally does not identify the hydrogens. The original formula $K_2MSbS_4$ (M = Zn, Cd) determined from single-crystal diffraction would imply a +4 oxidation state for the unique Sb. However, $Sb^{4+}$ has not been observed in solid-state compounds. Some compounds such as $Sb_2O_4$ with apparent $Sb^{4+}$ species actually contain mixed $Sb^{3+}$ and $Sb^{5+}$.[35] Therefore, the title compounds are likely to contain SH groups.

What evidence can we adduce for the presence of H atoms, specifically SH groups? The presence of the −SH group in the crystal structure is confirmed by FT-IR spectra, as shown in Figure 2a. The absorption peaks at 2540 cm$^{-1}$ for both
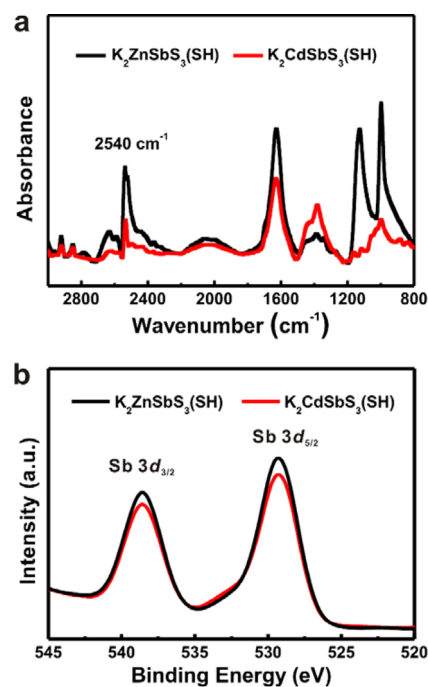


**Figure 2.** (a) FT-IR spectra of the $K_2MSbS_3(SH)$ (M = Zn, Cd) compounds. (b) XPS Sb 3d spectra of the $K_2MSbS_3(SH)$ (M = Zn, Cd) compounds.

compounds are attributed to the S−H stretching. They are comparable to the S−H stretching frequencies of ca. 2590 cm$^{-1}$ in thiols and cysteine.[36,37] Further evidence comes from calorimetry. Thermogravimetric analyses were also conducted for the title compounds (Figure S4). The onset temperatures of the weight loss of the two compounds are similar (∼390 °C). The weight losses (4.9% for $K_2ZnSbS_3(SH)$ and 4.1% for $K_2CdSbS_3(SH)$) correspond to the decompositions of the two compounds, releasing $H_2S$ (g). In addition, calculation of electron localization function (ELF) of $K_2ZnSbS_4$ (i.e., without

H atoms) using the tight binding linear muffin-tin orbital method[38−40] shows that there are attractors at the S4 site (the sulfur atom singly bonded to Zn) corresponding to the lone pairs of the sulfur atom (see Figure S5). These localized electron densities are attractors for the proton.

The XPS Sb 3d spectra of the two compounds are similar (Figure 2b), implying the Sb atoms have the same oxidation state. The peaks with binding energy of 538.6 and 529.3 eV correspond to the $3d_{3/2}$ and $3d_{5/2}$, respectively, of the $Sb^{3+}$ oxidation states.[41] Therefore, a charge balance is realized in $K_2MSbS_3(SH)$ (M = Zn, Cd) with classical oxidation states of K, M, Sb, S, and H as +1, +2, +3, −2, and +1, respectively. Furthermore, the bond valence sums of the cations, as shown in the Table S2 in Supporting Information, consists with the above oxidation states. Obviously, these are classical Zintl−Klemm compounds from the above experimental evidence.[42,43]

**Powder X-ray Diffraction and Optical Absorption.** The phase purity of the as-synthesized crystals was checked by powder X-ray diffraction (XRD), as illustrated in Figure 3. The
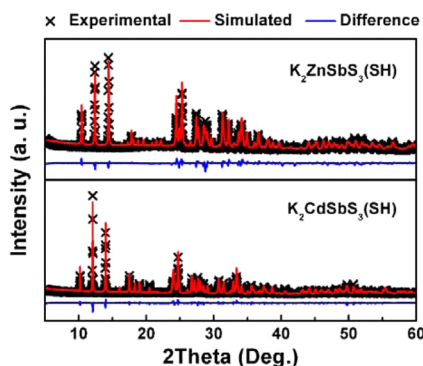


**Figure 3.** Powder XRD patterns of $K_2MSbS_3(SH)$ (M = Zn, Cd). The simulated patterns of are obtained by the *GSAS* program.

measured pattern of the two compounds matched well with their simulated ones obtained from single-crystal data. No extra peaks were observed. Note that the pattern of the $K_2CdSbS_3(SH)$ crystals slightly shifts to lower diffraction angles compared to that of $K_2ZnSbS_3(SH)$, due to the increase of the lattice constants.

The optical absorption properties of the two compounds were investigated by UV−vis diffuse reflectance spectroscopy (UV−vis) as depicted in Figure 4a. The sharp absorption edges of the two compounds, with onset wavelength around 450 nm, indicate their semiconductive nature. Remarkably, the absorption edges of $K_2ZnSbS_3(SH)$ and $K_2CdSbS_3(SH)$ are similar, consistent with the pale yellow colors of the crystals. An extrapolation method was used to determine the band gaps of the two semiconductors from the absorption spectra, as illustrated in Figure 4b. The optical band gap energies of $K_2ZnSbS_3(SH)$ and $K_2CdSbS_3(SH)$ are 2.75 and 2.71 eV, respectively.

The similar band gap energies of the two compounds indicate that the VBM and CBM mainly consist of S and Sb states and hence are not affected by the change of transition metal from Zn to Cd. Therefore, we propose an electronic structure model of $K_2CdSbS_3(SH)$ as shown in Figure 4c. The band gap of bulk CdS is 2.45 eV, with the electronic transition from S-3p to Cd-5s states. Different from that of the bulk CdS, the VBM of bulk $Sb_2S_3$ ($E_g$ = 1.7 eV) is mainly composed of S-3p and Sb-5s states. The band structures change to molecular
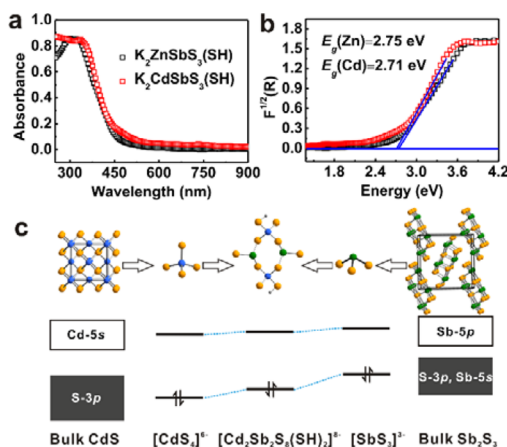


**Figure 4.** (a) Solid-state UV−vis absorption spectra of $K_2MSbS_3(SH)$ (M = Zn, Cd). (b) The plot of $F^{1/2}(R)$ vs energy by using the Kubelka−Munk equation for $K_2MSbS_3(SH)$ (M = Zn, Cd). (c) Schematic band structure of bulk CdS and $Sb_2S_3$ and HOMO and LUMO energy levels of $[CdS_4]^{6-}$, $[SbS_3]^{3-}$, and $[Cd_2Sb_2S_8(SH)_2]^{8-}$.

states when the dimension of the three-dimensional bulk binary compounds reduces to that of discrete clusters or chains. The highest occupied molecular orbital−lowest unoccupied molecular orbital (HOMO−LUMO) gap of $[CdS_4]^{6-}$ is larger than that of $[SbS_3]^{3-}$. Therefore, the combined clusters, namely, the $[Cd_2Sb_2S_8(SH)_2]^{8-}$ eight-membered rings, have a smaller HOMO−LUMO gap than that of the $[CdS_4]^{6-}$ tetrahedron but larger than that of $[SbS_3]^{3-}$ because of the participation of the higher Sb-5s states in the HOMO of the composite compound.

**Photoluminescence.** Photoluminescence excitation and emission spectra of $K_2CdSbS_3(SH)$ powder are shown in Figure 5a−c. When monitoring the emission intensity at 610
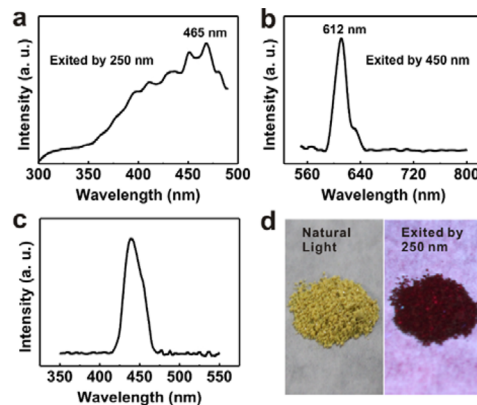


**Figure 5.** Emission spectra of $K_2CdSbS_3(SH)$ excited by 250 (a) and 550 (b) nm. (c) Excitation spectrum of $K_2CdSbS_3(SH)$. (d) Photographs of emission from $K_2CdSbS_3(SH)$ powder.

nm, we observed a peak around 450 nm (Figure 5c). The peak corresponds to the band gap of $K_2CdSbS_3(SH)$. On excitation at 250 nm, the strongest emission peak, centered at 465 nm (2.67 eV), appeared. This blue luminescence is attributed to the band edge emission of $K_2CdSbS_3(SH)$. On excitation at 450 nm (band edge), a new emission peak centered at 612 nm (2.03 eV) emerged, indicating that the compound may possess red light emission properties. Photographs of $K_2CdSbS_3(SH)$ powder under a 250 nm UV lamp are shown in Figure 5d.

Clearly, red luminescence was observed. This red emission of $K_2CdSbS_3(SH)$ is similar to that of $K_2Cd_3S_4$ (646 nm).[16]

**Electronic Structure Calculation.** DFT calculations of the two compounds were performed to understand the electronic band structure of these materials. The band structure and total density of states of $K_2CdSbS_3(SH)$ are shown in Figure 6. The
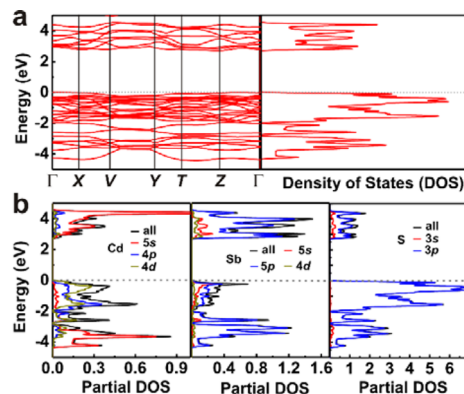


**Figure 6.** (a) Band structure (left) and total DOS (right) of $K_2CdSbS_3(SH)$. (b) Partial DOS of Cd, Sb, and S.

results show that the $K_2CdSbS_3(SH)$ compound has a band gap (Figure 6a). The band gap of 2.7 eV fits well with the UV−vis−NIR results for the compound. It is worthy to note that the band gap of $K_2CdSbS_3(SH)$ (1D, 2.71 eV) is similar to that of the two-dimensional compound $K_2Cd_3S_4$ (2.75 eV). Generally, the band gap of a material can be strongly influenced by the dimensionality of the materials and by the electronegativity difference between the cations and anions in the structure.[20] In comparison to $K_2Cd_3S_4$, $K_2CdSbS_3(SH)$ has a similar electronegativity difference between the cations and anion. It also has a lower dimensional sublattice, but even slightly smaller band gap. Furthermore, the band gap is not affected if the Cd sites are replaced by Zn. Therefore, the detailed band structure of $K_2CdSbS_3(SH)$ near Fermi surface is dominated by the Sb−S building blocks, but not the Cd−S building blocks.

The experimental optical absorption edges can be explained from the analyses of the total and partial density of states (DOS) in Figure 6b. Total and partial DOS of $K^+$ ions (Figure S6 in Supporting Information) make little contribution to the VBM and CBM. Cd-4d, Sb-5s, and S-3p states contribute to the VBM, while the CBM is mainly composed of Sb-5p states. The Cd-5s states, as proposed, are located in the bottom of the CB (ca. −4.5 eV, see Figure 6b), and make little contribution to the CBM.

The $K_2ZnSbS_3(SH)$ compound has a similar band structure as that of $K_2CdSbS_3(SH)$ (see Figure S7 in Supporting Information). The calculated band gap of $K_2ZnSbS_3(SH)$ is 2.6 eV, corresponding to the transition from S-3p and Sb-5s to Sb-5p states.

## CONCLUSION

In summary, we have successfully synthesized via the reactive flux method two new compounds of composition $K_2MSbS_3(SH)$ (M = Zn, Cd), which crystallize in the triclinic space group $P\bar{1}$. The presence of the SH group was confirmed by the FT-IR spectra and thermogravimetric analysis. The structures feature one-dimensional $\frac{1}{\infty}[M_2Sb_2S_6(SH_2)]^{4-}$ double chains, which are constructed by $[M_2Sb_2S_8(SH)_2]^{8-}$ eight-membered rings along the $a$ axis. Both compounds show sharp

absorption edges, ∼2.75 eV for $K_2ZnSbS_3(SH)$ and 2.71 eV for $K_2CdSbS_3(SH)$, indicating their semiconductive nature. DFT calculations, which fit well the experimental data, reveal that the Sb-5p states play an important role in constructing the CBM. $K_2CdSbS_3(SH)$ shows red emissions (612 nm) upon irradiation at room temperature. These two compounds offer an approach for the development of low-dimensional materials. Furthermore, the synthetic method also provides a new way to introduce SH groups in inorganic compounds.

## ASSOCIATED CONTENT

### ⓢ Supporting Information

The Supporting Information is available free of charge on the ACS Publications website at DOI: 10.1021/acs.inorgchem.6b01529.

> SEM, EDX, bond distances/angles, bond valence sums of $K_2MSbS_3(SH)$ (M = Zn, Cd), and electronic structure of $K_2ZnSbS_3(SH)$ (PDF)
> X-ray crystallographic information (CIF)

## AUTHOR INFORMATION

**Corresponding Authors**
*E-mail: jhlin@pku.edu.cn. (J.L.)
*E-mail: huangfq@pku.edu.cn. (F.H.)

**Notes**
The authors declare no competing financial interest.

## ACKNOWLEDGMENTS

## REFERENCES

(1) Zhang, X.; He, J.; Chen, W.; Zhang, K.; Zheng, C.; Sun, J.; Liao, F.; Lin, J.; Huang, F. *Chem. - Eur. J.* **2014**, *20*, 5977−5982.
(2) Zhang, X.; Chen, W.; Mei, D. J.; Zheng, C.; Liao, F. H.; Li, Y. T.; Lin, J. H.; Huang, F. Q. *J. Alloys Compd.* **2014**, *610*, 671−675.
(3) Liu, M.-L.; Chen, I. W.; Huang, F.-Q.; Chen, L.-D. *Adv. Mater.* **2009**, *21*, 3808−3812.
(4) Chan, G. H.; Liu, M.-L.; Chen, L.-D.; Huang, F.-Q.; Bugaris, D. E.; Wells, D. M.; Ireland, J. R.; Hersam, M. C.; Van Duyne, R. P.; Ibers, J. A. *Inorg. Chem.* **2008**, *47*, 4368−4374.
(5) Shi, X. Y.; Huang, F. Q.; Liu, M. L.; Chen, L. D. *Appl. Phys. Lett.* **2009**, *94*, 122103.
(6) Doussier-Brochard, C.; Chavillon, B.; Cario, L.; Jobic, S. *Inorg. Chem.* **2010**, *49*, 3074−3076.
(7) Takase, K.; Sato, K.; Shoji, O.; Takahashi, Y.; Takano, Y.; Sekizawa, K.; Kuroiwa, Y.; Goto, M. *Appl. Phys. Lett.* **2007**, *90*, 161916.
(8) Goto, Y.; Tanaki, M.; Okusa, Y.; Shibuya, T.; Yasuoka, K.; Matoba, M.; Kamihara, Y. *Appl. Phys. Lett.* **2014**, *105*, 022104.
(9) Hiramatsu, H.; Yanagi, H.; Kamiya, T.; Ueda, K.; Hirano, M.; Hosono, H. *Chem. Mater.* **2008**, *20*, 326−334.
(10) Inoue, S.; Ueda, K.; Hosono, H.; Hamada, N. *Phys. Rev. B: Condens. Matter Mater. Phys.* **2001**, *64*, 5.
(11) Pacquette, A. L.; Hagiwara, H.; Ishihara, T.; Gewirth, A. A. *J. Photochem. Photobiol., A* **2014**, *277*, 27−36.
(12) Zhang, X.; Liu, Y.; Zhang, G.; Wang, Y.; Zhang, H.; Huang, F. *ACS Appl. Mater. Interfaces* **2015**, *7*, 4442−4448.

(13) Repins, I.; Contreras, M. A.; Egaas, B.; DeHart, C.; Scharf, J.; Perkins, C. L.; To, B.; Noufi, R. *Prog. Photovoltaics* **2008**, *16*, 235−239.

(14) Trindade, T.; O'Brien, P.; Pickett, N. L. *Chem. Mater.* **2001**, *13*, 3843−3858.

(15) Duan, X. F.; Huang, Y.; Agarwal, R.; Lieber, C. M. *Nature* **2003**, *421*, 241−245.

(16) Axtell, E. A.; Hanko, J.; Cowen, J. A.; Kanatzidis, M. G. *Chem. Mater.* **2001**, *13*, 2850−2863.

(17) Papavassiliou, G. C.; Mousdis, G. A.; Koutselas, I.; Raptopoulou, C. P.; Terzis, A.; Kanatzidis, M. G.; Axtell, E. A. *Adv. Mater. Opt. Electron.* **1998**, *8*, 263−267.

(18) Axtell, E. A.; Liao, J. H.; Pikramenou, Z.; Kanatzidis, M. G. *Chem. - Eur. J.* **1996**, *2*, 656−666.

(19) Axtell, E. A.; Park, Y.; Chondroudis, K.; Kanatzidis, M. G. *J. Am. Chem. Soc.* **1998**, *120*, 124−136.

(20) Goodenough, J. B. *J. Phys. Chem. Solids* **1969**, *30*, 261−280.

(21) Ben Nasr, T.; Maghraoui-Meherzi, H.; Ben Abdallah, H.; Bennaceur, R. *Phys. B* **2011**, *406*, 287−292.

(22) Sunshine, S. A.; Kang, D.; Ibers, J. A. *J. Am. Chem. Soc.* **1987**, *109*, 6202−6204.

(23) Zhang, X.; Wang, Q.; Ma, Z.; He, J.; Wang, Z.; Zheng, C.; Lin, J.; Huang, F. *Inorg. Chem.* **2015**, *54*, 5301−5308.

(24) Meng, S.; Zhang, X.; Zhang, G.; Wang, Y.; Zhang, H.; Huang, F. *Inorg. Chem.* **2015**, *54*, 5768−5773.

(25) Wang, R.; Zhang, X.; He, J.; Zheng, C.; Lin, J.; Huang, F. *Dalton Trans.* **2016**, *45*, 3473−3479.

(26) Sheldrick, G. M. *SHELXTL NT*, Version 5.1, Program for Solution and Refinement of Crystal Structures; University of Göttingen: Germany, 1997.

(27) Larson, A. C.; Von Dreele, R. B. *General Structure Analysis System (GSAS) Los Alamos National Laboratory Report Laur* **2004**, 86−748.

(28) Kortüm, G.; Braun, W.; Herzog, G. *Angew. Chem., Int. Ed. Engl.* **1963**, *2*, 333−341.

(29) Kresse, G.; Hafner, J. *Phys. Rev. B: Condens. Matter Mater. Phys.* **1993**, *47*, 558−561.

(30) Kresse, G.; Furthmüller, J. *Comput. Mater. Sci.* **1996**, *6*, 15−50.

(31) Kresse, G.; Furthmüller, J. *Phys. Rev. B: Condens. Matter Mater. Phys.* **1996**, *54*, 11169−11186.

(32) Perdew, J. P.; Burke, K.; Ernzerhof, M. *Phys. Rev. Lett.* **1996**, *77*, 3865−3868.

(33) Blöchl, P. E. *Phys. Rev. B: Condens. Matter Mater. Phys.* **1994**, *50*, 17953.

(34) Klepp, K. O.; Bronger, W. *Rev. Chim. Miner* **1983**, *20*, 682−688.

(35) Amador, J.; Gutierrez Puebla, E.; Monge, M. A.; Rasines, I.; Ruiz Valero, C. *Inorg. Chem.* **1988**, *27*, 1367−1370.

(36) Manocha, A. S.; Fateley, W. G.; Shimanouchi, T. *J. Phys. Chem.* **1973**, *77*, 1977−1981.

(37) Qian, W.; Krimm, S. *Biopolymers* **1992**, *32*, 1503−1518.

(38) Andersen, O. K.; Jepsen, O. *Phys. Rev. Lett.* **1984**, *53*, 2571−2574.

(39) Andersen, O. K.; Pawlowska, Z.; Jepsen, O. *Phys. Rev. B: Condens. Matter Mater. Phys.* **1986**, *34*, 5253−5269.

(40) Nowak, H. J.; Andersen, O. K.; Fujiwara, T.; Jepsen, O.; Vargas, P. *Phys. Rev. B: Condens. Matter Mater. Phys.* **1991**, *44*, 3577−3598.

(41) Zakaznova-Herzog, V. P.; Harmer, S. L.; Nesbitt, H. W.; Bancroft, G. M.; Flemming, R.; Pratt, A. R. *Surf. Sci.* **2006**, *600*, 348−356.

(42) Zintl, E. *Angew. Chem.* **1939**, *52*, 1−6.

(43) Nesper, R. *Z. Anorg. Allg. Chem.* **2014**, *640*, 2639−2648.